Supercooled Goldstone Bosons at the QCD Chiral Phase Transition

Adrien Florio,[1,2,*] Eduardo Grossi,[3,†] Aleksas Mazeliauskas,[4,‡] Alexander Soloviev,[5,§] and Derek Teaney[6,∥]
[1]*Fakultät für Physik, Universität Bielefeld, D-33615 Bielefeld, Germany*
[2]*Department of Physics, Brookhaven National Laboratory, Upton, New York 11973-5000, USA*
[3]*Dipartimento di Fisica, Università di Firenze and INFN Sezione di Firenze, via G. Sansone 1, 50019 Sesto Fiorentino, Italy*
[4]*Institut für Theoretische Physik, Universität Heidelberg D-69120 Heidelberg, Germany*
[5]*Faculty of Mathematics and Physics, University of Ljubljana, Jadranska ulica 19, SI-1000 Ljubljana, Slovenia*
[6]*Center for Nuclear Theory, Department of Physics and Astronomy, Stony Brook University, New York, New York 11794-3800, USA*

(Received 1 July 2025; revised 10 October 2025; accepted 12 November 2025; published 12 December 2025)

We discuss a universal nonequilibrium enhancement of long-wavelength Goldstone bosons induced by quenches to the broken phase in Model G—the dynamical universality class of an $O(4)$ antiferromagnet and the chiral phase transition in QCD. Scaling arguments for the coarsening dynamics describing the formation of the chiral condensate predict a parametric enhancement in the infrared spectra of Goldstone bosons, a prediction confirmed by stochastic simulations of the transition. The details of the enhancement are determined by the nonlinear dynamics of a superfluid effective theory, which is a limit of Model G reflecting the broken $O(4)$ symmetry. Our results translate to a parametric enhancement of low-momentum pions in heavy-ion collisions at the LHC, which are underpredicted in current hydrodynamic models without critical dynamics.

DOI: 10.1103/wyn4-ncdc

Introduction—Experiments at the Relativistic Heavy Ion Collider (RHIC) and the Large Hadron Collider (LHC) have provided compelling evidence that high-energy heavy-ion collisions create an extended space-time region of quark-gluon plasma (QGP) [1]. QGP is the high-temperature phase of quantum chromodynamics (QCD) where the approximate chiral symmetry of the QCD Lagrangian is restored [2]. As the QGP rapidly expands and cools, the system returns to the hadronic phase, where quarks and gluons are confined and chiral symmetry is spontaneously broken. This transition is a smooth crossover [3,4] but lies close in parameter space to a second-order critical point. In the chiral limit, where the up and down quark masses vanish, the transition is second order [5–8] and believed to belong to the universality class of an $O(4)$ antiferromagnet. Near this critical point, both the correlation length ξ and the relaxation time $\tau_R \propto \xi^\zeta$ grow, giving rise to universal dynamics. As the QCD medium expands and cools, this universal dynamics controls both the formation of the chiral condensate (the order parameter of the chiral transition) and the production of soft pions (the Goldstone modes of the transition).

Many years ago the dynamical universality class of chiral QCD was identified as "Model G" in the classification scheme of Halperin and Hohenberg [9]. Early studies speculated that the rapid expansion of the QGP could lead to the formation of a disoriented chiral condensate [9–12], but these predictions were never experimentally confirmed [13–16]. In the intervening years, hydrodynamic models for heavy-ion collisions achieved remarkable success in describing the bulk properties of these collisions, placing tight constraints on QGP transport properties [1]. Nevertheless, a persistent tension between hydro models and increasingly precise data on the yield of low-momentum pions suggests that the hydrodynamic description of the QGP is incomplete [17–24]. Moreover, recent progress in lattice QCD has highlighted the significance of the $O(4)$ critical point to real-world QCD, reviving interest in chiral critical dynamics and its potential phenomenological signatures [25–33].

With this context, we study the coarsening dynamics describing the formation of the chiral condensate after a quench from the restored to the broken phase in Model G. Because of distinctive reversible couplings (i.e., Poisson brackets) between the $O(4)$ order parameter and QCD's conserved charges, coarsening in this model is markedly different from other previously studied critical models such as Model A and Model B [34,35]. Indeed, these couplings cause the Goldstone modes to behave like pseudoparticles that propagate ballistically over many correlation lengths before diffusing back into the medium. This separation of

*Contact author: aflorio@physik.uni-bielefeld.de
†Contact author: eduardo.grossi@unifi.it
‡Contact author: a.mazeliauskas@thphys.uni-heidelberg.de
§Contact author: alexander.soloviev@fmf.uni-lj.si
∥Contact author: derek.teaney@stonybrook.edu

scales leads to a parametric enhancement over equilibrium of the infrared spectrum Goldstone bosons, which persists after the quench for a parametrically long time compared to τ_R. We verify these predictions through comprehensive stochastic simulations of instantaneous quenches in Model G, described in detail in our companion paper [36]. The soft pion enhancement is a rigorous prediction of QCD close to the chiral phase transition, and it is a prediction with tantalizing phenomenological implications.

$O(4)$ *antiferromagnet (Model G)*—We briefly review Model G [37] and refer the reader to our companion paper [36] and previous works [27]. Model G captures the dynamics of an $O(4)$ local order parameter $(\phi_0, \phi_1, \phi_2, \phi_3)$ coupled to partially conserved axial charges n_A^ℓ and conserved vector charges n_V^ℓ, which can be combined in an antisymmetric $O(4)$ tensor n_{ab} with $n_{0\ell} = n_A^\ell$ and $n_{\ell_1\ell_2} = \epsilon^{\ell_1\ell_2\ell} n_V^\ell$. In equilibrium, the fields are distributed according to the following Landau-Ginzburg free energy:

$$\mathcal{H}[\phi] = \int d^3x \left[\frac{1}{2}\nabla\phi_a \cdot \nabla\phi_a + U(\phi) + \frac{1}{4\chi_I} n_{ab} n^{ab}\right], \quad \text{(1a)}$$

$$U(\phi) = \frac{1}{2} m_0^2 \phi^2 + \frac{\lambda}{4}(\phi \cdot \phi)^2. \quad \text{(1b)}$$

The dynamics is governed by the following equations of motion (EoM):

$$\partial_t \phi_a + \frac{1}{\chi_I} n_{ab}\phi_b = \Gamma_0 \frac{\delta\mathcal{H}}{\delta\phi_a} + \theta_a, \quad \text{(2a)}$$

$$\partial_t n_{ab} + \nabla \cdot (\nabla\phi_{[a}\phi_{b]}) = \sigma_0 \nabla^2 \frac{\delta\mathcal{H}}{\delta n_{ab}} + \partial_i \Xi^i_{ab}. \quad \text{(2b)}$$

The left-hand side of Eq. (2) has a Poisson bracket structure and encodes the ideal superfluid dynamics discussed below. The right-hand side encodes the dissipative dynamics with the relaxation coefficient Γ_0 and conductivity σ_0. Finally, the noise terms, θ and Ξ, reproduce the fluctuation-dissipation theorem.

At fixed coupling λ, the model has a critical mass m_c^2; for example, for $\lambda = 4$, $m_c^2 = -4.811$ [30,38]. For $m_0^2 > m_c^2$, the $O(4)$ symmetry remains unbroken, and the mean value of the order parameter ϕ_a (the chiral condensate in QCD) vanishes. For $m_0^2 < m_c^2$, the $O(4)$ symmetry is spontaneously broken to $O(3)$, producing a condensate, $\langle\phi_a\rangle \equiv \bar{\sigma}_{\mathrm{eq}} n_a$ (with $n_a n_a = 1$), and three pion Goldstone modes $\vec{\pi}(t, \boldsymbol{x}) = (\pi_1, \pi_2, \pi_3)$ describing the fluctuations of $\phi_a(t, \boldsymbol{x})$ orthogonal to n_a and the direction of $\phi_a(t, \boldsymbol{x})$.

In the broken phase, the magnitude of the order parameter ϕ_a is approximately constant, and the left-hand side of Eq. (2) describes the coupling between conserved charges and Goldstone modes. When the dissipative terms are neglected, the resulting coupled equations correspond to an ideal non-Abelian superfluid, reflecting the breaking of $O(4)$ symmetry [26,39]. The ideal superfluid theory depends on just two parameters: $f^2 = \phi_a\phi_a$ and the susceptibility χ_I, both of which can be determined from Euclidean measurements in lattice QCD [40–42].

A linearized analysis of the superfluid equations (including dissipation) yields the pion dispersion relation $\omega(k) = vk - iD_A k^2/2$ with $v^2 = f^2/\chi_I$ [43]. Thus, the propagation of long-wavelength pions is characterized by two timescales: a "ballistic" timescale $1/(vk)$ and a "diffusive" timescale $1/(D_A k^2)$.

Even near the critical point, these timescales remain parametrically separated for $k\xi \ll 1$. Matching the hydrodynamic pion effective field theory (EFT) to the underlying critical theory gives $v \sim \xi^{(2-d)/2} \sim \xi/\tau_R$, where ξ is the diverging correlation length and $\tau_R \sim \xi^{d/2}$ is the relaxation time of the order parameter [44]. Meanwhile, the diffusion constant scales as $D_A \sim \xi^2/\tau_R$ [43].

Thus for large systems with $L \gg \xi$ and $k \sim 1/L$, there are two parametrically separated timescales:

$$t_B \equiv \frac{L}{v} \sim \tau_R \left(\frac{L}{\xi}\right) \quad \text{(3)}$$

and

$$t_D \equiv \frac{L^2}{D_A} \sim \tau_R \left(\frac{L}{\xi}\right)^2, \quad \text{(4)}$$

and the hierarchy $\tau_R \ll t_B \ll t_D$ holds near the critical point. As we will see, when the system undergoes an instantaneous quench from the symmetric to the broken phase, the hierarchy of timescales leads to a strong enhancement of the infrared spectrum of the Goldstone modes (pions).

Quenches and scaling analysis—We consider the setup shown in Fig. 1. The system begins in thermal equilibrium at $T > T_c$ ($m_0^2 > m_c^2$, red-dashed potential) and is suddenly quenched into the broken phase at $T < T_c$ ($m_0^2 < m_c^2$, blue potential), with the quench tuned so that the correlation length ξ remains the same before and after the quench. The postquench field configuration is unstable. In a region of

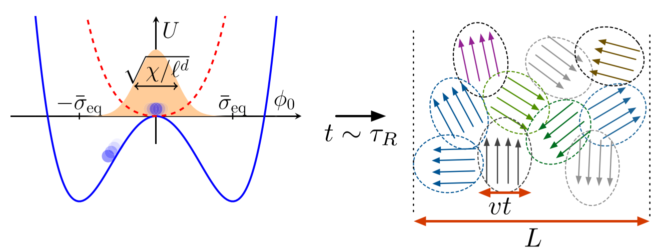

FIG. 1. Illustration of instantaneous quenches in Model G. Left: at every point in space, the effective potential of the theory suddenly changes from a convex potential to a double-well potential. After a time of order τ_R, the field locally reaches a new minimum in field space, leading to many small randomly oriented domains shown in the right panel. Right: the domains merge in a time $t_B \sim L/v$ with coarsening dynamics given by the superfluid limit of Model G (see text).

size ℓ (several correlation lengths long), fluctuations of the locally averaged order parameter $\bar{\phi}_a$ are of order $\sim\sqrt{\chi/\ell^d}$, where $\chi \sim \xi^{2-\eta}$ is the chiral susceptibility. These fluctuations seed the instability, and the local order parameter finds a new equilibrium value $\bar{\sigma}_{\text{eq}} \sim \xi^{-(d-2+\eta)/2}$ on a short timescale $\sim\tau_R$. At this point, many small, randomly oriented domains have formed. On a longer timescale $t \sim L/v$, these domains begin to grow and merge. Since this growth time $t_B \sim L/v$ is much longer than the relaxation time τ_R, the superfluid (hydrodynamic) limit of Model G provides an appropriate dynamical description of the condensate growth. We will now elaborate on this picture.

As a proxy for the global condensate, we focus on "magnetization" $M_a(t) = \phi_a(t, \boldsymbol{k} = 0)$, which is the zeroth mode of the Fourier transformed order parameter $\phi_a(t, \boldsymbol{k}) \equiv (1/V)\sum_{\boldsymbol{x}} e^{-i\boldsymbol{k}\cdot\boldsymbol{x}}\phi_a(t, \boldsymbol{x})$. In addition, we consider the three pion fields $\pi^\ell(t, \boldsymbol{k})$, which are projections of $\phi_a(t, \boldsymbol{k})$ orthogonal to M_a. In particular, we study the nonequilibrium evolution of the following equal-time two-point correlation functions:

$$G_0(t) \equiv \frac{V}{4}\sum_{a=1}^{4}\langle M_a(t) M_a(t)\rangle, \tag{5}$$

$$G_{\pi\pi}(t, \boldsymbol{k}) \equiv \frac{V}{3}\sum_{\ell=1}^{3}\langle \pi^\ell(t, \boldsymbol{k})\pi^\ell(t, -\boldsymbol{k})\rangle. \tag{6}$$

Our companion paper details these definitions [36].

At late times, when the quasiparticle approximation is valid, the classical pion fields can be treated as fluctuations around a global condensate,

$$(\sqrt{\chi_I}/\bar{\sigma}_{\text{eq}})\pi^\ell(t, \boldsymbol{x}) \simeq \sum_{\boldsymbol{k}} a^\ell_{\boldsymbol{k}} e^{-i\omega(k)t + i\boldsymbol{k}\cdot\boldsymbol{x}}/\sqrt{2\omega(k)V} + \text{c.c.} \tag{7}$$

The leading factor $\sqrt{\chi_I}/\bar{\sigma}_{\text{eq}}$ canonically normalizes the pion field to match the quasiparticle description [36]. Then, $\chi_I G_{\pi\pi}(t, k)/\bar{\sigma}^2_{\text{eq}} \simeq n_\pi(t, k)/\omega(k)$ estimates the soft-pion yield, $n_\pi(t, k) = \sum_\ell \langle |a^\ell_{\boldsymbol{k}}|^2\rangle/3$. Below we will compare $G_{\pi\pi}$ to equilibrium, $G_{\pi\pi}/G^{\text{eq}}_{\pi\pi} \simeq n_\pi(t, k)/n^{\text{eq}}_\pi(k)$, finding a soft-pion enhancement postquench. In the future, the stochastic field configurations at late times can be precisely matched onto a Boltzmann description [26].

In Fig. 2, we provide a qualitative summary of the nonequilibrium time evolution of $G_{\pi\pi}(t, k)$ based on the following scaling discussion of $G_0(t)$ and then $G_{\pi\pi}(t, k)$. At early times, the order parameter forms small domains in a time $\sim\tau_R$. Domain alignment and the accompanying magnetization growth take place over the ballistic timescale $t_B \gg \tau_R$, i.e. the time needed to propagate across the volume. Finally, when the magnetization equilibrates $M_a \sim \bar{\sigma}_{\text{eq}} n_a$, $G_0(t)$ approaches $V\bar{\sigma}^2_{\text{eq}}/4 \sim \xi^{2-\eta}(L/\xi)^d$. Having identified the timescales and asymptotes, we formulate a scaling form

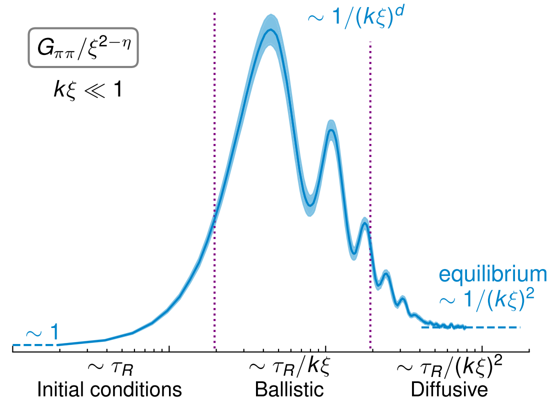

FIG. 2. Schematic time evolution of the pion-pion correlator $G_{\pi\pi}(t, k)$ at small momenta $k\xi \ll 1$, following a symmetric quench at $t = 0$ from the restored to the broken phase in three dimensions ($d = 3$). The system first relaxes locally for $t \sim \tau_R$, seeding local condensate domains and setting the initial conditions for correlator growth. Pions of size $1/k \gg \xi$ then propagate ballistically over time $t \sim \tau_R/(k\xi) \sim 1/vk$, and the condensate domains grow to size $\sim 1/k$. This coarsening dynamics in $d = 3$ enhances $G_{\pi\pi}$ by $\sim 1/k\xi$ over equilibrium $G^{\text{eq}}_{\pi\pi} \sim \xi^{2-\eta}/(k\xi)^2$. Finally, the pion correlator returns to equilibrium (the dashed line) via diffusion for $t \sim \tau_R/(k\xi)^2$.

for the nonequilibrium evolution of the correlation function G_0 for intermediate times $\tau_R \ll t \sim t_B \ll t_D$:

$$G_0(t, \xi, L) = \xi^{2-\eta}(L/\xi)^d \mathcal{F}(vt/L, \xi/L). \tag{8}$$

So far, since $v \sim \xi/\tau_R$, this is a simple rewrite of the usual statement of the dynamical scaling hypothesis, where all times are scaled by $\tau_R \propto \xi^\zeta$ and all lengths are scaled by ξ. Now, however, for $L \to \infty$ and vt/L fixed, we expect $\mathcal{F}$ to be a regular function as $\xi/L \to 0$ and the ξ/L dependence can be dropped:

$$G_0(t, \xi, L) = \xi^{2-\eta}(L/\xi)^d \mathcal{F}(vt/L). \tag{9}$$

This is a scaling prediction for the nonequilibrium evolution of condensate growth. In an overlap region between early and ballistic times $\tau_R \ll t \ll t_B$, G_0 must be independent of system volume, so $\mathcal{F}(vt/L) \propto (vt/L)^d$ and the magnetization grows as a power law, $G_0 \propto \xi^{2-\eta}(t/\tau_R)^d$.

We have identified a significant time region $\tau_R \ll t \sim t_B \ll t_D$, where the condensate grows significantly following a quench. Since the relevant times $t \gg \xi/v$ are large compared to the relaxation time τ_R, this is a hydrodynamic regime with locally broken symmetry. However, dissipation does not become important until late times $t \sim t_D$. Therefore, the appropriate hydrodynamic description is given by the ideal superfluid equations discussed above. In the future, these superfluid equations can be simulated directly to determine condensate growth. Although similar to coarsening in other critical systems [35], the linear growth of domain size in time uniquely reflects the superfluid limit of Model G.

A similar scaling analysis can be applied to the pion correlation function $G_{\pi\pi}(t,k)$ in (6). Consider a regime where $\xi \ll 1/k \sim L$. For times $t \lesssim t_B$, all four components of $\phi_a(t,\boldsymbol{k})$ are uncorrelated and should behave similarly [see Fig. 1(b)]. We therefore expect the pion correlator to scale similarly to G_0, though the numerical result depends on kL, $G_{\pi\pi}(t,\xi,k,L) = \xi^{2-\eta}(L/\xi)^d \mathcal{F}(vkt, kL)$. Here, in analogy with (9), the residual $k\xi \ll 1$ dependence has been dropped, while keeping $vkt \sim 1$ fixed. In an overlap region, $1/L \ll k \ll 1/\xi$, the correlation function must become volume independent and we expect that $\mathcal{F}(vkt, kL)$ simplifies to $\mathcal{F}(vkt)/(kL)^d$. Thus, in infinite volume, the time evolution of the soft pion correlator takes a simple nonequilibrium scaling form

$$G_{\pi\pi}(t,\xi,k) = \xi^{2-\eta}(k\xi)^{-d}\mathcal{F}(vkt) \tag{10}$$

for the extended temporal range $\tau_R \ll t \sim t_B \ll t_D$.

The scaling arguments can also be extended to a small but finite pion mass m, incorporating explicit symmetry breaking. The scaling form becomes $G_{\pi\pi}(t,\xi,k,L,m) = \xi^{2-\eta}(L/\xi)^d\mathcal{F}(vmt, kL, mL)$. Assuming that $\mathcal{F}$ is volume independent for momenta such that $1/L \ll k \ll m \ll 1/\xi$ immediately implies that

$$G_{\pi\pi}(t,\xi,k,m) = \xi^{2-\eta}(m\xi)^{-d}\mathcal{F}(vmt). \tag{11}$$

The effects of the nonequilibrium dynamics are striking. Noting that the late-time equilibrium pion correlator is $G^{\rm eq}_{\pi\pi}(\xi,k) \sim \xi^{2-\eta}/[(k\xi)^2 + (m\xi)^2]$ [27], Eqs. (10) and (11) imply a parametric enhancement over the equilibrium values for $d = 3$:

$$\frac{G_{\pi\pi}(t,k)}{G^{\rm eq}_{\pi\pi}(k)} \underset{t\sim 1/vk}{\sim} \begin{cases} 1/k\xi, & k \gg m \\ 1/m\xi, & k \ll m \end{cases}. \tag{12}$$

This is the key result of our analysis. We predict that during sudden quenches to the broken phase, the infrared spectrum of Goldstone bosons (pions) is parametrically enhanced relative to equilibrium for a significant period of time, $\tau_R \ll t \sim t_B \ll t_D$; see Fig. 2.

Numerical simulations—The scaling predictions can be tested by numerical simulations of (2a) and (2b). The details are reported in the accompanying work [36]. In Figs. 3 and 4, we confirm the nonequilibrium time evolution from our dynamic scaling analysis of the magnetization and pion correlation functions. Figure 3 shows the evolution of the condensate, estimated from $\sqrt{\langle M^2\rangle}$, following an instantaneous symmetric quench from t_r^0 to $-\mathsf{t}_\mathsf{r}^0$. Here $\mathsf{t}_\mathsf{r} \equiv (m_0^2 - m_c^2)/|m_c^2|$ is the reduced temperature and the correlation lengths in these quenches scale as $\xi \sim |\mathsf{t}_\mathsf{r}|^{-\nu}$ with $\nu = 0.7377(41)$ [45]. Our scaling analysis is confirmed by the data collapse in the lower panel, where time is scaled by the ballistic time $t_B = L/v$ and the

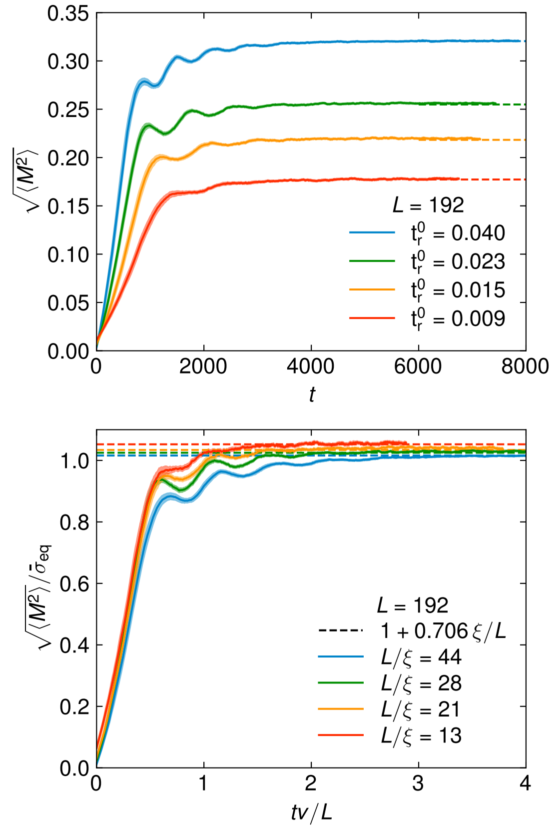

FIG. 3. The chiral condensate (estimated by $\sqrt{\langle M_a M_a\rangle}$) versus time following a symmetric quench, $\mathsf{t}_\mathsf{r}^0 \to -\mathsf{t}_\mathsf{r}^0$, for several reduced temperatures t_r^0. The upper panel shows the raw data, while the lower panel shows the data with the x and y axes rescaled by L/v and $\bar{\sigma}_{\rm eq}$, respectively. The data collapse [up to $\xi(\mathsf{t}_\mathsf{r})/L$ corrections] confirms the nonequilibrium scaling predictions of (9).

condensate is scaled by $\bar{\sigma}_{\rm eq}$. Violations from scaling come from finite volume corrections which distinguish $\sqrt{\langle M_a M_a\rangle}$ from $\bar{\sigma}_{\rm eq}$ [45]. [In practice, the finite-size corrections to the magnetization can be parametrized as $\sqrt{\langle M_a M_a\rangle_{\rm eq}} \approx \bar{\sigma}_{\rm eq}(1 + 0.706\xi/L)$ [36].]

The nonequilibrium evolution of $G_{\pi\pi}(t,k)$ is shown in Fig. 4. The top panel shows the raw data for quenches with different initial t_r^0 at fixed $k = 2\pi/L$. Quench temperatures starting farther from T_c have smaller ξ and corresponding $k\xi$, and are more enhanced. After rescaling time with vk and the pion correlator with $k\xi/G^{\rm eq}_{\pi\pi}$, the data show good collapse for $1 \lesssim tvk \lesssim 4$, confirming the nonequilibrium scaling in (10) and implying a soft-pion enhancement. After the initial growth, $G_{\pi\pi}$ relaxes slowly toward equilibrium on a diffusive timescale t_D, and the nonequilibrium scaling no longer applies.

Much more can be said about the dynamics of instantaneous quenches. We refer the reader to the accompanying paper for additional results on the evolution of fluctuations parallel to M_a (the sigma) and detailed mean-field computations of $G_0(t)$ and $G_{\pi\pi}(t,k)$ [36].

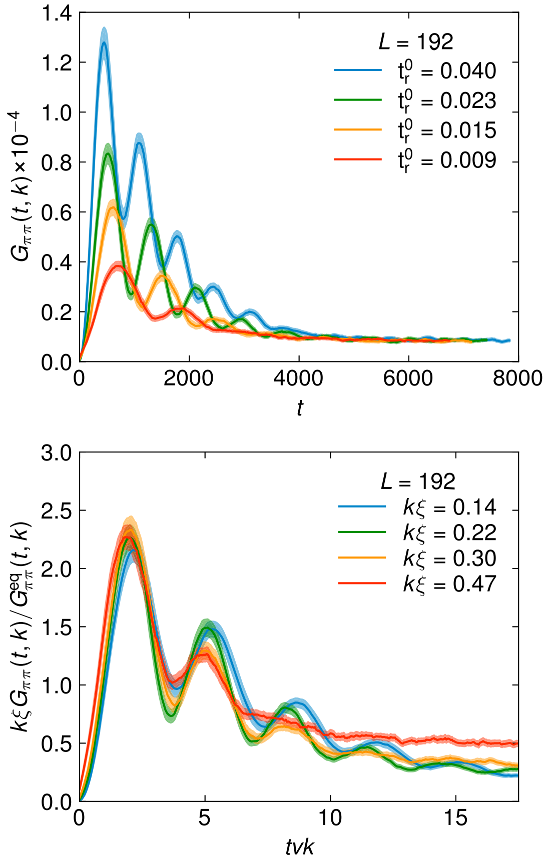

FIG. 4. Pion-pion correlator versus time at $k = 2\pi/L$ following a symmetric quench $\mathfrak{t}_r^0 \to -\mathfrak{t}_r^0$ for several initial reduced temperatures $\mathfrak{t}_r^0$. The upper panel shows the raw data, while the lower panel shows the data with the x and y axes rescaled by vk and $k\xi/G^{\mathrm{eq}}_{\pi\pi}$, respectively. The data collapse at intermediate times in the lower panel supports the nonequilibrium scaling in (10) and implies that $G_{\pi\pi}(t,k)$ is parametrically enhanced by $\sim 1/k\xi$ at these times. At late times, the scaled correlators thermalize and the scaled correlators do not collapse.

Discussion—The chiral phase transition in QCD spontaneously breaks $O(4) \simeq SU(2)_L \times SU(2)_R$ symmetry below T_c. The dynamic critical behavior describing the transition between the restored and broken phases (which resembles the transition between a normal and superfluid) belongs to the universality class of Model G [37]. Below T_c the hydrodynamic description in the chiral limit incorporates the Goldstone modes (the pions), forming a non-Abelian superfluid [39].

For the case of instantaneous quenches to the broken phase, we use generic scaling arguments and explicit numerical simulations to understand the nonequilibrium dynamics of two-point correlation functions and condensate growth following a quench (see also the companion paper [36]). The key result of our analysis is that at intermediate ballistic times, the infrared spectrum of the pion correlation function is parametrically enhanced over its equilibrium expectation; see Eq. (12).

Preliminary work shows that this qualitative prediction is robust to explicit symmetry breaking, i.e., a small pion mass. We have also relaxed the quench setup by sweeping the temperature through the phase transition at a finite rate, and we are finding similar results. If real-world QCD lies outside the $O(4)$ scaling window [31,46], exhibiting only broken chiral symmetry and a moderately light pseudo-Goldstone mode, the qualitative reasons for the enhanced pion yield remain intact. Indeed, as described above (see Fig. 1), the condensate growth and the pion enhancement are driven by the superfluid dynamics of the pion EFT, after being seeded with random small domains induced by the quench. Critical scaling determines the temperature dependence of the EFT parameters and the initial domain size and is essential for the data collapse seen in Fig. 4. But the enhancement is more general, requiring only some random seeds and the applicability of the hydrodynamic pion EFT (with some parameters) at later times.

These results should be a strong motivation for future heavy-ion experiments, such as ALICE3 [47], to carefully measure the yield and correlations of low momentum pions with p_T of order the pion mass. Of immediate relevance is the current measured yield of soft pions, which rises above baseline hydrodynamic expectations for $p_T \lesssim 400$ MeV and reaches a $\sim 50\%$ enhancement near $p_T \sim m_\pi$ [24]. A key difficulty for current hydrodynamic models, which currently do not include the dynamics of chiral symmetry breaking, is the lack of a soft momentum scale that would produce a deviation from equilibrium only at small momentum.

Our simulations are an idealization of heavy ion collisions and real-world QCD. Here we considered only instantaneous quenches in the chiral limit, noting that these simplifying features can be relaxed in future studies [48]. Our Letter is part of a broader effort to understand the universal properties of nonequilibrium critical systems. However, the analysis naturally explains why low-momentum pions should be preferentially enhanced relative to equilibrium, provided the expansion of a heavy ion collision through the chiral transition is sufficiently rapid and the real-world pion mass is sufficiently light. An essential next step is to implement the stochastic Model G dynamics within realistic hydrodynamic codes and with pion masses and chiral parameters motivated by lattice QCD and other studies [5,31,41,46]. This would quantify whether the nonequilibrium critical dynamics analyzed rigorously here (in a specific setup and limit of QCD) can account for the observed low p_T excess in heavy ion collisions.

Acknowledgments—We would like to thank Jürgen Berges, Jean-Paul Blaizot, Kirill Boguslavski, Jannis Gebhard, Alexander Kalweit, Govert Nijs, Thimo Preis, Klaus Reygers, Thomas Schäfer, Wilke van der Schee, Dam T. Son, and Urs Wiedemann for helpful discussions. This work is supported by the DFG through Emmy Noether Programme [Projects No. 545261797 (A. F.) and No. 496831614 (A. M.)] and through CRC 1225

ISOQUANT [Project No. 27381115 (A. M.)]. A. S. was supported by funding from Horizon Europe research and innovation programme under the Marie Skłodowska-Curie Grant Agreement No. 101103006 and the Project N1-0245 of Slovenian Research Agency (ARIS). This work was supported by the U.S. Department of Energy, Office of Science, Office of Nuclear Physics, Grant No. DE-SC0012704 (A. F.) and Grant No. DE-FG-02-88ER40388 (D. T.). This research used resources of the National Energy Research Scientific Computing Center (NERSC), a Department of Energy Office of Science User Facility using NERSC Award No. NP-ERCAP0028307. We thank ECT* (the European Centre for Theoretical Studies in Nuclear Physics and Related Areas) for support at the workshop "Attractors and thermalization in nuclear collisions and cold quantum gases," where we profited from helpful discussions.

Data availability—The data and plotting routines used in the figures are available at [49].

[1] W. Busza, K. Rajagopal, and W. van der Schee, Heavy ion collisions: The big picture, and the big questions, Annu. Rev. Nucl. Part. Sci. **68**, 339 (2018).

[2] R. D. Pisarski and F. Wilczek, Remarks on the chiral phase transition in chromodynamics, Phys. Rev. D **29**, 338 (1984).

[3] S. Borsanyi, Z. Fodor, J. N. Guenther, S. K. Katz, K. K. Szabo, A. Pasztor, I. Portillo, and C. Ratti, Higher order fluctuations and correlations of conserved charges from lattice QCD, J. High Energy Phys. 10 (2018) 205.

[4] A. Bazavov *et al.* (HotQCD Collaboration), Chiral crossover in QCD at zero and non-zero chemical potentials, Phys. Lett. B **795**, 15 (2019).

[5] H. T. Ding *et al.* (HotQCD Collaboration), Chiral phase transition temperature in $(2+1)$-flavor QCD, Phys. Rev. Lett. **123**, 062002 (2019).

[6] O. Kaczmarek, F. Karsch, A. Lahiri, L. Mazur, and C. Schmidt, QCD phase transition in the chiral limit, NIC Ser. **50**, 193 (2020).

[7] A. Y. Kotov, M. P. Lombardo, and A. Trunin, QCD transition at the physical point, and its scaling window from twisted mass Wilson fermions, Phys. Lett. B **823**, 136749 (2021).

[8] F. Cuteri, O. Philipsen, and A. Sciarra, On the order of the QCD chiral phase transition for different numbers of quark flavours, J. High Energy Phys. 11 (2021) 141.

[9] K. Rajagopal and F. Wilczek, Static and dynamic critical phenomena at a second order QCD phase transition, Nucl. Phys. **B399**, 395 (1993).

[10] J. D. Bjorken, A full acceptance detector for SSC physics at low and intermediate mass scales: An expression of interest to the SSC, Int. J. Mod. Phys. A **07**, 4189 (1992).

[11] J.-P. Blaizot and A. Krzywicki, Soft pion emission in high-energy heavy ion collisions, Phys. Rev. D **46**, 246 (1992).

[12] S. Gavin, A. Gocksch, and R. D. Pisarski, How to make large domains of disoriented chiral condensate, Phys. Rev. Lett. **72**, 2143 (1994).

[13] G. Arnison *et al.* (UA1 Collaboration), Search for Centauro like events at the CERN proton anti-proton collider, Phys. Lett. **122B**, 189 (1983).

[14] G. J. Alner *et al.* (UA5 Collaboration), An accelerator search at 900 GeV CM energy for the Centauro phenomenon, Phys. Lett. B **180**, 415 (1986).

[15] C. R. A. Augusto, S. L. C. Barroso, V. Kopenkin, M. Moriya, C. E. Navia, and E. H. Shibuya, Search for disoriented chiral condensate in cosmic γ-hadron families, Phys. Rev. D **59**, 054001 (1999).

[16] T. C. Brooks *et al.* (MiniMax Collaboration), A search for disoriented chiral condensate at the Fermilab Tevatron, Phys. Rev. D **61**, 032003 (2000).

[17] B. Abelev *et al.* (ALICE Collaboration), Centrality dependence of π, K, p production in Pb-Pb collisions at $\sqrt{s_{NN}} = 2.76$ TeV, Phys. Rev. C **88**, 044910 (2013).

[18] S. Acharya *et al.* (ALICE Collaboration), Production of charged pions, kaons, and (anti)protons in Pb-Pb and inelastic pp collisions at $\sqrt{s_{NN}} = 5.02$ TeV, Phys. Rev. C **101**, 044907 (2020).

[19] A. Mazeliauskas and V. Vislavicius, Temperature and fluid velocity on the freeze-out surface from π, K, p spectra in pp, p-Pb and Pb-Pb collisions, Phys. Rev. C **101**, 014910 (2020).

[20] I. Melo and B. Tomášik, Kinetic freeze-out in central heavy-ion collisions between 7.7 and 2760 GeV per nucleon pair, J. Phys. G **47**, 045107 (2020).

[21] D. Devetak, A. Dubla, S. Floerchinger, E. Grossi, S. Masciocchi, A. Mazeliauskas, and I. Selyuzhenkov, Global fluid fits to identified particle transverse momentum spectra from heavy-ion collisions at the Large Hadron Collider, J. High Energy Phys. 06 (2020) 044.

[22] G. Nijs, W. van der Schee, U. Gürsoy, and R. Snellings, Bayesian analysis of heavy ion collisions with the heavy ion computational framework trajectum, Phys. Rev. C **103**, 054909 (2021).

[23] D. Everett *et al.* (JETSCAPE Collaboration), Multisystem Bayesian constraints on the transport coefficients of QCD matter, Phys. Rev. C **103**, 054904 (2021).

[24] P. Lu, R. Kavak, A. Dubla, S. Masciocchi, and I. Selyuzhenkov, Quantification of the low-p_T pion excess in heavy-ion collisions at the LHC and top RHIC energy, Nucl. Sci. Tech. **36**, 142 (2025).

[25] S. Schlichting, D. Smith, and L. von Smekal, Spectral functions and critical dynamics of the O(4) model from classical-statistical lattice simulations, Nucl. Phys. B **950**, 114868 (2020).

[26] E. Grossi, A. Soloviev, D. Teaney, and F. Yan, Transport and hydrodynamics in the chiral limit, Phys. Rev. D **102**, 014042 (2020).

[27] E. Grossi, A. Soloviev, D. Teaney, and F. Yan, Soft pions and transport near the chiral critical point, Phys. Rev. D **104**, 034025 (2021).

[28] X. Cao, M. Baggioli, H. Liu, and D. Li, Pion dynamics in a soft-wall AdS-QCD model, J. High Energy Phys. 12 (2022) 113.

[29] L. H. Yao and U. C. Täuber, Critical dynamics of the antiferromagnetic O(3) nonlinear sigma model with conserved magnetization, Phys. Rev. E **105**, 064128 (2022).

[30] A. Florio, E. Grossi, and D. Teaney, Dynamics of the O(4) critical point in QCD: Critical pions and diffusion in Model G, Phys. Rev. D **109**, 054037 (2024).

[31] J. Braun *et al.*, Soft modes in hot QCD matter, Phys. Rev. D **111**, 094010 (2025).

[32] J. V. Roth, Y. Ye, S. Schlichting, and L. von Smekal, Dynamic critical behavior of the chiral phase transition from the real-time functional renormalization group, J. High Energy Phys. 01 (2025) 118.

[33] J. V. Roth, Y. Ye, S. Schlichting, and L. von Smekal, Universal critical dynamics near the chiral phase transition and the QCD critical point, Phys. Rev. D **111**, L111901 (2025).

[34] A. J. Bray, Theory of phase-ordering kinetics, Adv. Phys. **43**, 357 (1994).

[35] U. Täuber, *Critical Dynamics: A Field Theory Approach to Equilibrium and Non-Equilibrium Scaling Behavior* (Cambridge University Press, Cambridge, England, 2014).

[36] A. Florio, E. Grossi, A. Mazeliauskas, A. Soloviev, and D. Teaney, companion paper, Quenching through the QCD chiral phase transition, Phys. Rev. D **112**, 114019 (2025).

[37] P. C. Hohenberg and B. I. Halperin, Theory of dynamic critical phenomena, Rev. Mod. Phys. **49**, 435 (1977).

[38] A. Florio, E. Grossi, A. Soloviev, and D. Teaney, Dynamics of the $O(4)$ critical point in QCD, Phys. Rev. D **105**, 054512 (2022).

[39] D. T. Son, Hydrodynamics of nuclear matter in the chiral limit, Phys. Rev. Lett. **84**, 3771 (2000).

[40] A. Bazavov *et al.*, Meson screening masses in $(2+1)$-flavor QCD, Phys. Rev. D **100**, 094510 (2019).

[41] M. Cè, T. Harris, A. Krasniqi, H. B. Meyer, and C. Török, Aspects of chiral symmetry in QCD at $T = 128$ MeV, Phys. Rev. D **107**, 054509 (2023).

[42] A. Krasniqi, M. Cè, R. J. Hudspith, and H. B. Meyer, Hot QCD matter around the chiral crossover: A lattice study with O(a)-improved Wilson fermions, Phys. Rev. D **110**, 114506 (2024).

[43] D. T. Son and M. A. Stephanov, Real time pion propagation in finite temperature QCD, Phys. Rev. D **66**, 076011 (2002).

[44] D. T. Son and M. A. Stephanov, Pion propagation near the QCD chiral phase transition, Phys. Rev. Lett. **88**, 202302 (2002).

[45] J. Engels and F. Karsch, Finite size dependence of scaling functions of the three-dimensional O(4) model in an external field, Phys. Rev. D **90**, 014501 (2014).

[46] J. Braun, W.-j. Fu, J. M. Pawlowski, F. Rennecke, D. Rosenblüh, and S. Yin, Chiral susceptibility in $(2+1)$-flavor QCD, Phys. Rev. D **102**, 056010 (2020).

[47] ALICE Collaboration, Letter of intent for ALICE 3: A next-generation heavy-ion experiment at the LHC, arXiv:2211.02491.

[48] A. Florio, E. Grossi, A. Mazeliauskas, A. Soloviev, and D. Teaney, in progress.

[49] A. Florio, E. Grossi, A. Mazeliauskas, A. Soloviev, and D. Teaney, Plotting routines and data files for 2504.03514 and 2504.03516, 2025, 10.5281/zenodo.17600429.